SUSTAINABLE ENGINEERING

(eISSN:3083-8231)
Article
Volume 2, Issue 1, 2025
https://doi.org/10.51200/susten.v2i1.5052

Ultrahydrophobic Surface for Water Treatment by Membrane Processes-Prediction of Water Contact Angle on Air/Solid Composite Surface by Solving Young-Laplace Equation

Takeshi Matsuura

Department of Chemical and Biological Engineering, University of Ottawa, 161 Louis Pasteur, Ottawa ON, K1N 6N5, CANADA.
*Correspondence: matsuura@uottawa.ca

*ORCID ID:0000-0002-1461-7904
Received: 02.05.2024, Accepted: 03.12.2024

Abstract: The evaluation of contact angle (CA) of air-solid composite surface is growing in its importance in membrane separation technology. The reason is that the super-hydrophobic property of the surface allows self-cleaning of membrane surface in various membrane separation processes and also mitigates pore wetting, which is considered the serious disadvantage of membrane distillation. The Cassie-Baxter equation is currently considered one of the best tools to evaluate CA of the air-solid composite surface. However, most of the experimental works of CA measurement were carried out by the sessile drop method, in which the size of the droplet is limited to micro- or submicrometer range, and it is not known how CA is affected by the air content of the air-solid composite surface especially when the droplet size is in a range of millimeter. In this work, the meniscus shape of a large water droplet with a size greater than the capillary length (2.713 mm) was calculated for different air contents at the air-solid surface by solving the Young-Laplace differential equation. It was concluded that the effect of f_s (fraction of solid surface) on CA does not depend significantly on the droplet size, even though the droplet flattens considerably as the droplet size increases.

Keywords: Contact angle; Cassie-Baxter equation; Young-Laplace equation

© 2025 by UMS Press.

1. Introduction

The enhancement of CA on a rough surface has attracted much attention in recent years. For example, the self-cleaning property of the plant leaves, called lotus effect [1], is being mimicked in the design of synthetic membranes.

It is also well known the air trapped in the grooves of a rough membrane surface makes the surface ultra-hydrophobic and prevents water from entering the membrane pore. This phenomenon is utilised to mitigate pore wetting of membranes for membrane distillation [2].

The surface of any rough solid has a greater CA than a smooth surface, meaning that the experimentally measurable CA, called the apparent CA, is greater than the ideal CA, called Young CA, which applies to smooth solid surfaces. The Young equation was adapted by

Wenzel and then Cassie-Baxter to relate these two CAs with each other, depending on the state of surface wetting (Figure 1) [3,4].

Wenzel proposed the following equation (1) [3], where r is a unitless surface roughness factor that expresses the degree of surface heterogeneity [5]. θ_Y and θ_W are, respectively, the Young and apparent contact angle (°).

$$\cos\theta_W = r\cos\theta_Y \quad (1)$$

Cassie and Baxter, on the other hand, attempted to extend Wenzel's analysis to rough porous surfaces [6]. The simplified version of their model for water is given by the following equation (2) [3]:

$$\cos\theta_{CB} = f_s(\cos\theta_Y + 1) - 1 \quad (2)$$

where θ_{CB} is the apparent CA (°) and f_s is the fraction of solid surface which is in contact with the liquid water.

In the Cassie and Baxter model, water contacts only the solid surface, and the grooves (pores) are completely water-free and filled with air. Since air is superhydrophobic with a CA of 180°, the CA of the air-solid composite surface becomes greater than the CA of the solid.

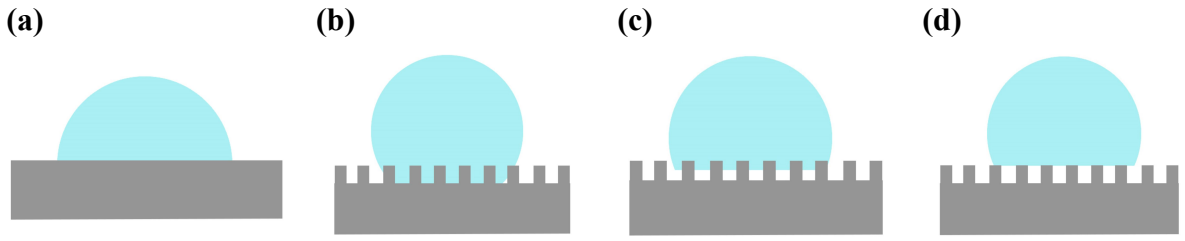

Figure 1. Schematic of surface wettability on ideal or rough surfaces according to the (a) Young, (b) Wenzel, (c) intermediate, and (d) Cassie-Baxter equations, adapted and redrawn from [3].

Due to the growing importance of the surface modification to prevent the surface wetting, there is continued interest in revisiting the Cassie-Baxter equation to propose new ways of its derivation or modifications [7,8]. An overview of the Cassie-Baxter equation is also available in [9].

It should also be reminded that the experimental measurement of CA is carried out in most cases by the sessile drop method where droplets of micrometer or semi-micrometer size are used to avoid the gravity effects, and under such circumstances, the droplet shape is approximately spherical. A question will then arise, how CA is affected by the surface morphology when the droplet size is so large that its meniscus shape is no longer spherical under the gravity effect. This question is crucial, as droplets in millimeter or even centimeter range are frequently observed in real life.

Although the effect of gravity on the CA has been discussed in some studies [10-12], these works did not consider the influence of surface morphology. Tang et al. [13] is the only one

that addresses both surface morphology and gravity effects on CA. However, the pillar size used in their paper as the parameter for the microstructure is limited to nanometer range.

The objective of this work is to examine how CA is affected by the air content of the air-solid composite surface especially when the droplet size is as large as few millimeters. To this end, the Young-Laplace differential equation is solved to draw computationally the shape of the water droplet on a rough surface and then determine the CA at the edge of the droplet. For water, it is generally accepted that droplets larger than the capillary length of 2.713 mm have a non-spherical shape [14]. In this work, meniscus widths is stretched to more than five times the capillary length, and the CA of such large droplet is determined computationally.

2. Materials and Methods

2.1 Using Circular Geometry: Applicable only when the size of the droplet is much smaller than capillary length l = 2.713 mm

When the size of the water droplet is smaller than the capillary length, the droplet can be assumed as a sphere cap (or a circular segment in 2D) as shown in Figure 2.

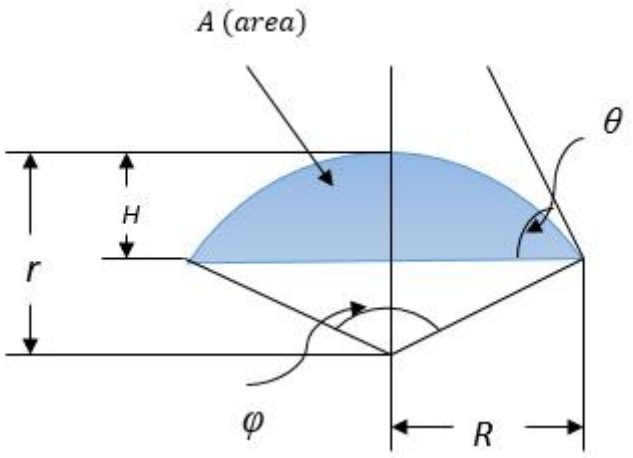

Figure 2. Droplet (blue colored) shape as a circular segment

In the figure:

$$\varphi = 2\theta \tag{3}$$

$$R = r\sin\theta \tag{4}$$

$$H = r(1-\cos\theta) \tag{5}$$

The area of the circular segment, A, is:

$$A = \frac{r^2}{2}(\varphi - \sin\varphi) \tag{6}$$

Using these relationships, the contact angle, θ, as a function of solid fraction, f_s, is calculated by the following steps:

a. A set of $R(1)$ and $\theta(1)$ for a circular segment on a 100 % solid surface (f_s =1) is chosen.
b. $H(1)$ and $A(1)$ of the above circular segment are calculated as follows:

$$r(1) = \frac{R(1)}{\sin\theta(1)} \tag{7}$$

From equation (5) and (6):

$$H(1) = \frac{R(1)}{\sin\theta(1)}(1 - \cos\theta(1)) \tag{8}$$

and

$$A(1) = \frac{1}{2}\left(\frac{R(1)}{\sin\theta(1)}\right)^2 (2\theta(1) - \sin 2\theta(1)\ ) \tag{9}$$

c. When there is no solid on the floor (f_s = 0), the floor is formed only with air, whose contact angle $\theta(0)$ is 180°. Then, the water droplet becomes a sphere (a circle in 2D). The circle's area, $A(0)$ is now set equal to $A(1)$, and the height of the circle, $H(0)$, is calculated by:

$$H(0) = 2\sqrt{\frac{A(1)}{\pi}} \tag{10}$$

d. $H(f_s)$ for a given value of f_s ($0 < f_s < 1$) is now calculated as a weighted average of $H(1)$ and $H(0)$:

$$H(f_s) = f_s H(1) + (1 - f_s)H(0) \tag{11}$$

$A(f_s)$ remains equal to $A(1)$.

Then, similar to equations (8) and (9):

$$H(f_s) = \frac{R(f_s)}{\sin\theta(f_s)}(1 - \cos\theta(f_s)) \tag{12}$$

$$A(f_s) = A(1) = \frac{1}{2}\left(\frac{R(f_s)}{\sin\theta(f_s)}\right)^2 (2\theta(f_s) - \sin 2\theta(f_s)\ ) \tag{13}$$

By solving equations (12) and (13) simultaneously, $R(f_s)$ and $\theta(f_s)$ can be obtained as a function of f_s.

2.2 Solving the Young-Laplace Differential Equation

It is known that the shape of a sessile droplet on a horizontal plate can be obtained by solving the Young-Laplace equation:

$$\frac{\frac{d^2h}{dr^2}}{\left(1+\left(\frac{dh}{dr}\right)^2\right)^{3/2}} + \frac{\frac{dh}{dr}}{r\left(1+\left(\frac{dh}{dr}\right)^2\right)^{1/2}} - \frac{2}{b} = \frac{h}{\left(\frac{\sigma}{\rho g}\right)} \tag{14}$$

Where r and h are the distance from the origin in r and h coordinate (see Figure. 3). σ, ρ and g are the surface tension of water, density of water and gravity constant, and b is equal to $1/(d^2h/dr^2)$ (at $r = 0$) [15].

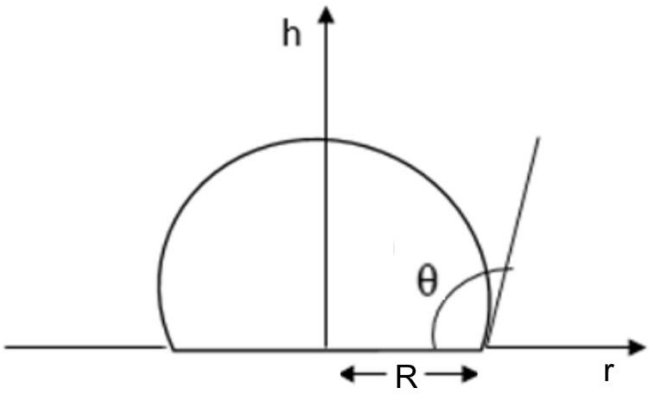

Figure 3. The shape of a sessile drop on a horizontal plate

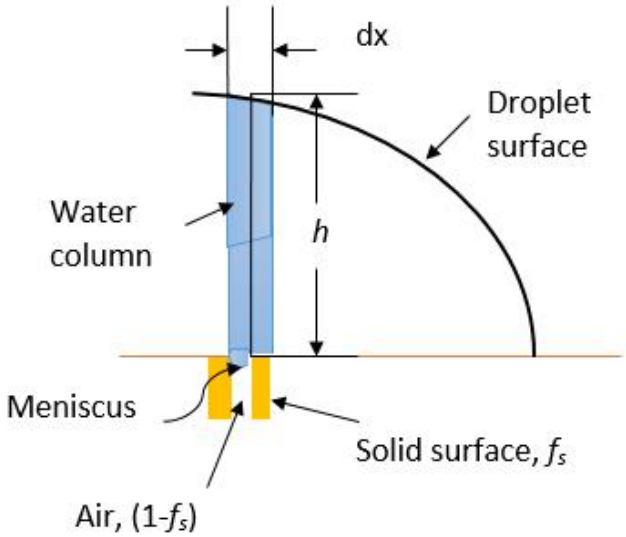

Figure 4. A segment of water droplet formed above an air filled pore and a piece of solid material

We assume a porous plate where infinitesimally small length, *dx,* in which air-filed pore and solid plate are placed side by side (see Figure. 4). Then, the weight of the water pillar on the air-filled pore is supported by the capillary pressure formed by the meniscus at the bottom of the water pillar and does not contribute to the balance between surface tension and weight of the water pillar. On the other hand, the weight of the liquid pillar above the solid plate, given by $\rho g h$ contributes fully to the balance.

When the fraction of the solid plate is f_s , the gravitational force $f_s \rho g h$ is balanced by the surface tension in segment *dx*. Then, the following equation applies instead of equation (14):

$$\frac{\frac{d^2h}{dr^2}}{\left(1+\left(\frac{dh}{dr}\right)^2\right)^{3/2}} + \frac{\frac{dh}{dr}}{r\left(1+\left(\frac{dh}{dr}\right)^2\right)^{1/2}} - \frac{2}{b} = \frac{h}{\left(\frac{\sigma}{f_s \rho g}\right)} \tag{15}$$

where $b = 1/(d^2h/dr^2)\ (\text{at } r = 0)$ [15].

By normalising:

$$\frac{\frac{d^2y}{dx^2}}{\left(1+\left(\frac{dy}{dx}\right)^2\right)^{3/2}} + \frac{\frac{dy}{dx}}{x\left(1+\left(\frac{dy}{dx}\right)^2\right)^{1/2}} - \frac{2}{b} = f_s y \tag{16}$$

Where x and y are $x = r/l$ and $y = h/l$ (see Figure 3 for r and h), respectively, and b is equal to $1/(d^2y/dx^2)\ (\text{at } x = 0)$. $l = \sqrt{\sigma/\rho g}$ = 2.713 x10^{-3} m is called the capillary length, as mentioned earlier.

CA for a given f_s , $\theta(f_s)$ is obtained as follows:

a. A set of $R(1)/l$ and $\theta(1)$ for a 100 % solid surface (f_s =1) is chosen. (see Figure 2 for R and θ)

b. Equation (16) is solved with the boundary conditions :

$$\frac{dy}{dx} = 0 \qquad \text{at } x = 0 \tag{17}$$

$$\frac{dy}{dx} = -\tan\theta \qquad \text{at } x = R(1)/l \tag{18}$$

The Bézier curve method is used to solve the differential equation [10,11] as shown in Appendix.

$H(1)/l$ can be obtained as the height of the drawn meniscus and the area, $A(1)/l^2$, is calculated by

$$A(1)/l^2 = 2\int_0^{R(1)/l} y dx \tag{19}$$

c. $H(0)/l$ is calculated by equation (20), similar to equation (10).

$$H(0)/l = 2\sqrt{\frac{A(1)/l^2}{\pi}} \tag{20}$$

d. For a given f_s , $(0 < f_s < 1)$ $H(f_s)/l$ is calculated by the following equation (21) and $A(f_s)/l^2$ is set eqal to $A(1)/l^2$.

e.

$$H(f_s)/l = f_s H(1)/l + (1 - f_s)H(0)/l \tag{21}$$

f. Equation (16) is solved by the Bézier curve method, but this time the boundary conditions are

$$\frac{dy}{dx} = 0 \qquad \text{at } x = 0 \tag{22}$$

$$y = \frac{H(f_s)}{l} \qquad \text{at } x = 0 \tag{23}$$

with the restriction

$$A(f_s)/l^2 = 2\int_0^{R(fs)/l} y dx = A(1) \tag{24}$$

From the drawn meniscus shape, $R(f_s)/l$ and $\theta(f_s)$ are obtained as a function of f_s. The computation was prrformed using Microsoft Excel.

3. Results and Discussion

3.1. Using Circular Geometry

a. $R(1)$ and $\theta(1)$ were chosen as 1.1747×10^{-3} m and 60°, respectively.
b. $H(1)$ and $A(1)$ were calculated by equations (8) and (9) as 0.6783×10^{-3} m and 1.1302 $\times 10^{-6}$ m^2, respectively.
c. $H(0)$ is calculated by equation (10) as 1.1996×10^{-3} m
d. $H(f_s)$ becomes

$$H(f_s) = f_s \times 0.6783 \times 10^{-3} + (1 - f_s) \times 1.1996 \times 10^{-3} \text{ m}$$

$$A(f_s) = A(1) = 1.1302\ 10^{-6} \text{m}^2$$

$\theta(f_s)$ and $R(f_s)$ were calculated for various values of f_s and the results are shown in in the 2nd column of Table 1 and 2.

Table 1. θ versus f_s obtained by different methods

f_s	θ, degree			
	Circular geometry	**Solving Young-Laplace equation**		**Cassie-Baxter equation**
		***R*(1)/*l* = 0.433**	***R*(1)/*l* = 5**	
1.0	60	60	60	60
0.8	78	72.9	72.4	78.5
0.5	107.2	104	103.2.	104.5
0.3	128.3	116	120.2	123
0.0	180	180	180	180

Table 2. $R(f_s)/l$ versus f_s obtained by different methods

f_s	$R(f_s)/l$		
	Circular geometry[a]	**Solving Young-Laplace equation**	
		***R*(1)/*l* = 0.433**	***R*(1)/*l* = 5**
1.0	0.433	0.433	5
0.8	0.356	0.364	4.11
0.5	0.254	0.247	2.98
0.3	0.186	0.186	2.31
0	0	0	0

[a] $R(f_s)$ was divided by l (= 2.713 x 10^{-3} m) and shown as $R(f_s)/l$.

The meniscus so obtained is shown for each f_s in Figure 5.

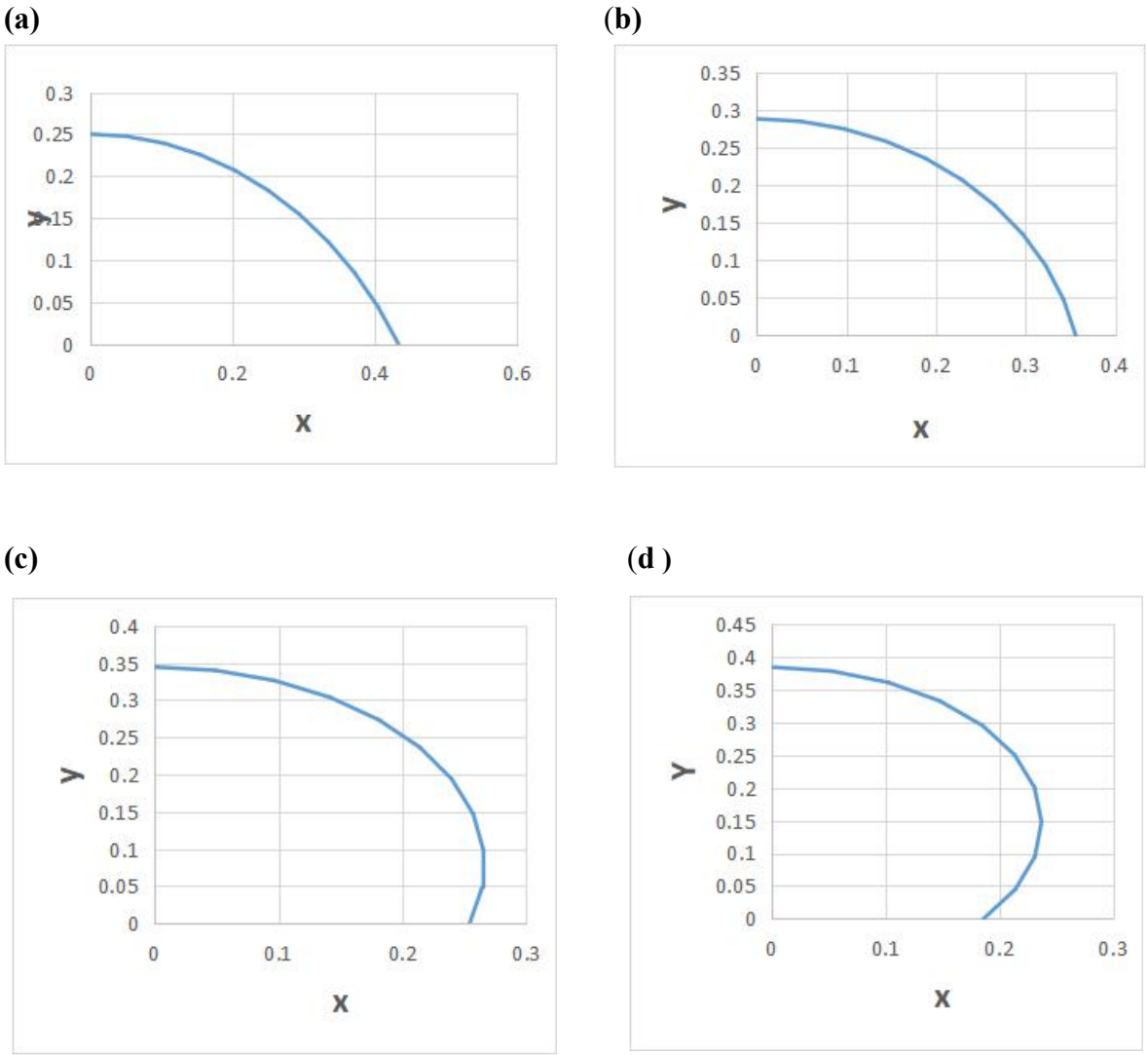

Figure 5. Meniscus shape for f_s = a) 1.0, b) 0.8, c) 0.5 and d) 0.3 (Circular geometry)

3.2. Solving the Young-Laplace Differential Equation

3.2.1 When R(1)/l < 1

a. $R(1)/l$ and $\theta(1)$ for a 100 % solid surface (f_s =1) were chosen to be 0.433 and 60°, respectively. Note that $R(1)/l$ is less than 1; therefore the droplet shape is approximated by a sphere (a circle for 2D).
b. Solving the Young-Laplace equation, $H(1)/l$ and $A(1)/l^2$ were obtained as 0.250 and 0.079677.
c. $H(0)/l$ was calculated using equation (20) to be 0.45.
d. $H(f_s)/l$ is calculated by:

$$H(f_s)/l = f_s \times 0.250 + (1 - f_s) \times 0.450$$

$$\frac{A(f_s)}{l^2} = \frac{A(1)}{l^2} = 0.079677$$

e. The differential equation (16) was solved for different values of f_s with boundary conditions (22) and (23), with the restriction of equation (24). From the meniscus shape, $\theta(f_s)$ and $R(f_s)/l$ were obtained, and the results are reported in the 3rd column of Tables 1 and 2.

3.2.2 When R(1)/l > 1

a. $R(1)/l$ and $\theta(1)$ for a 100 % solid surface (f_s =1) were chosen to be 5 and 60°, respectively. Note that $R(1)/l$ is more than 1, therefore the droplet shape cannot be approximated by a sphere (a circle for 2D).
b. Solving the Young-Laplace equation, $H(1)/l$ and $A(1)/l^2$ were obtained as 1.20 and 4.563797.
c. $H(0)/l$ was calculated using equation (20) to be 2.4106.
d. $H(f_s)/l$ is calculated by

$$H(f_s)/l = f_s \times 1.20 + (1 - f_s) \times 2.4106$$

e. The differential equation (16) was solved for different values of f_s with boundary conditions (22) and (23) with the restriction of equation (24). From the meniscus shape, $\theta(f_s)$ and $R(f_s)/l$ were obtained, and the results are reported in the 4th column of Tables 1 and 2.

The meniscus shapes obtained for each f_s are shown in Figure 6.

3.3 By Cassie-Baxter Equation

θ which is now called θ_{CB}, is calculated by equation (2), and the results are shown in the last column of Table 1.

3.4 Discussions

Looking into Table 1, the results from the circular geometry are mathematically rigorous. When these results are compared with those of Cassie-Baxter equation, CA was 2.7° higher for f_s = 0.5 and 5.3° higher for f_s = 0.3.

The results for $R(1)/l$ = 0.433 should agree with those for circular geometry since the droplet size is smaller than the capillary length l in this case. However, the former values are lower than the latter, with a deviation as high as 12.3° at f_s = 0.3, indicating inaccuracy of the solution of the differential equation by the cubic Bésier function. Perhaps accuracy could be improved by employing a higher order Bésier function.

Interestingly, the CA for $R(1)/l$ = 5 is much closer to the results for the Cassie-Baxter equation, with a maximum deviation of of 6.1° at f_s = 0.8.

(a) f_s = 1.0

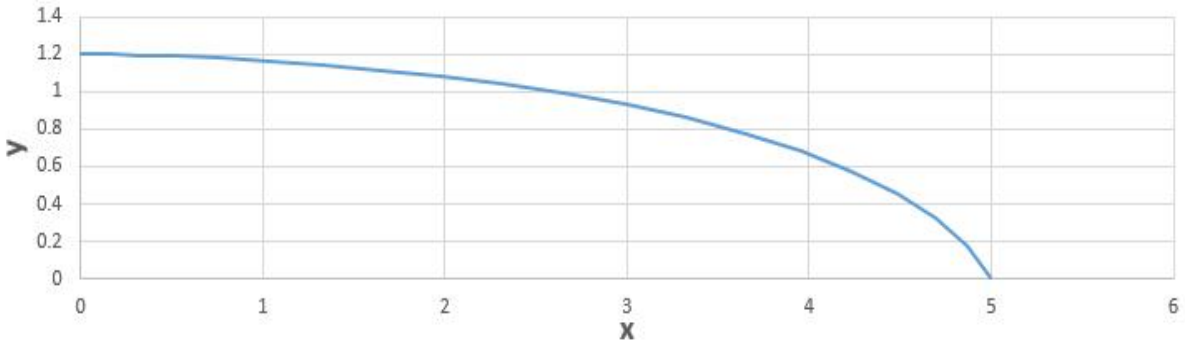

(b) f_s = 0.8

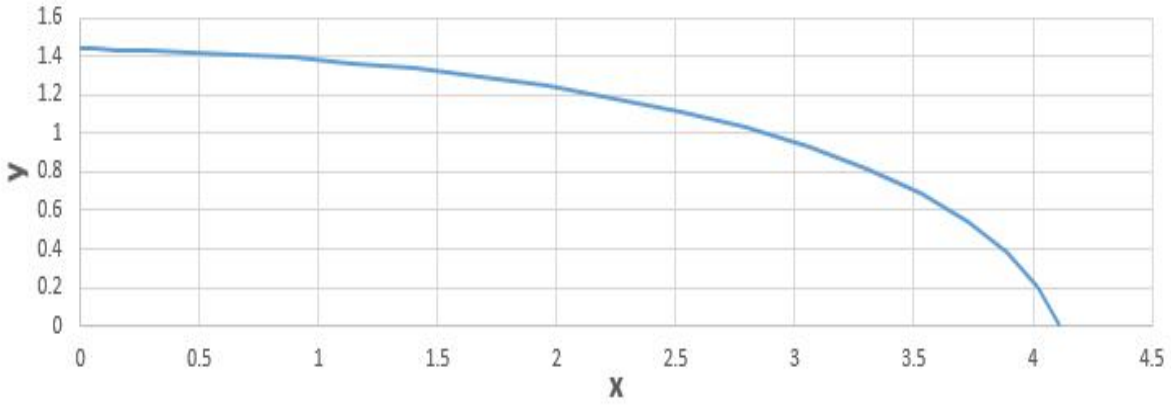

(c) f_s = 0.5

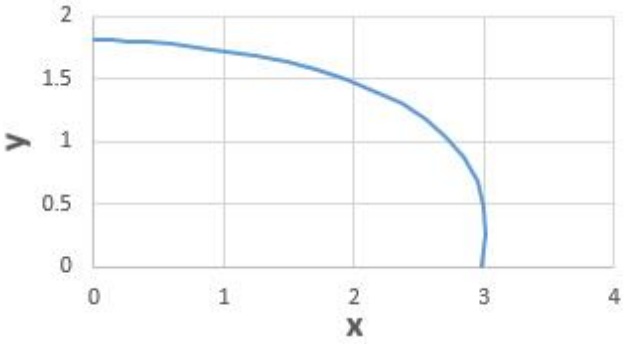

(d) f_s=0.3

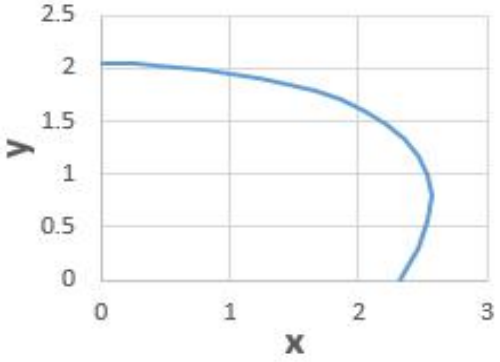

Figure 6. Meniscus shape for f_s = a) 1.0, b) 0.8, c) 0.5 and d) 0.3 (When $R(1)/l = 5$)

When all the CA data were plotted versus f_s in Figure 7, a single line was drawn with small scatters the along the line. On the other hand, when Figures 5 and 6 are compared, the circular segments shown in Figure 5 are considerably flattened in Figure 6 due to the gravity effect on the large droplet.

From these figures, it can be concluded that the effect of f_s (fraction of solid surface) on CA does not depend significantly on the droplet size, even though the droplet flattens considerably as the droplet size increases. It should be noted that the effect of the droplet size

on CA is known in the literature, i.e. CA changes with size due to the gravity effect [16]. However, we are reporting the first theoretical study concerning the effect of f_s on CA for different droplet sizes, which needs to be experimentally validated.

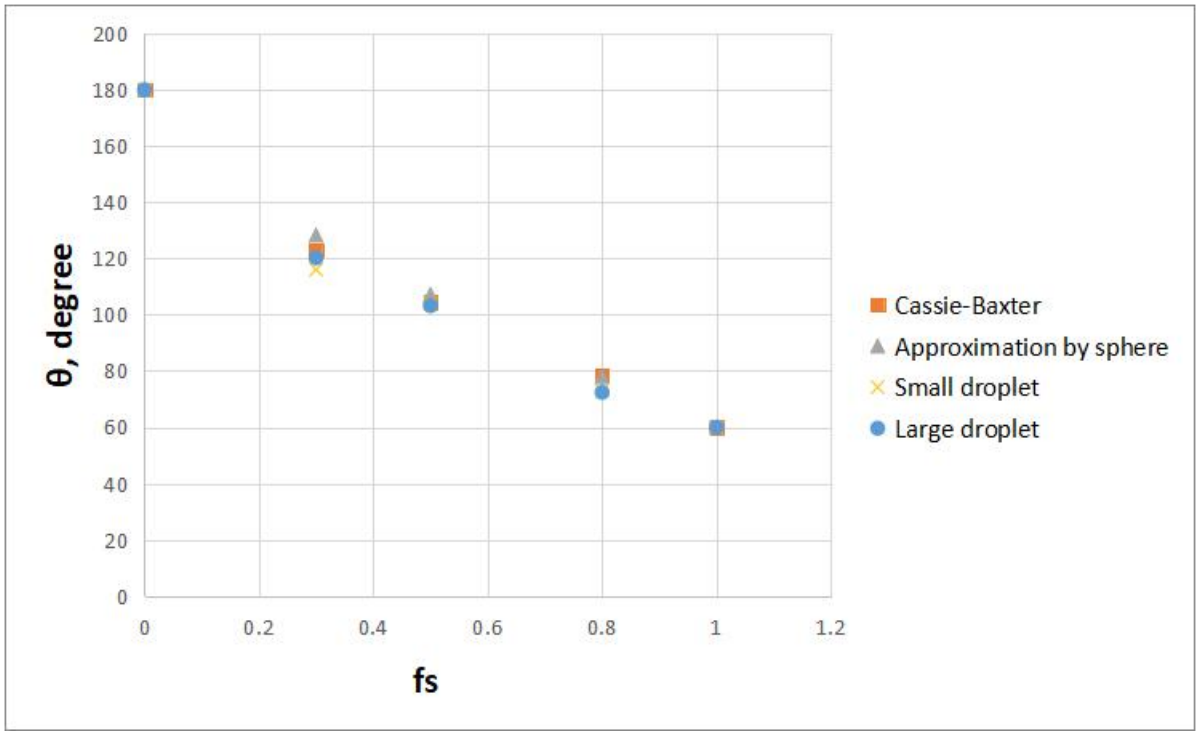

Figure 7. θ versus f_s obtained by various methods

Further looking into Table 2, $R(f_s)/l$ values for the circular geometry and those for $R(1)/l$ = 0.433 are almost the same. This indicates that CA is more sensitive to errors caused by the approximation in solving the differential equation than $R(f_s)/l$.

4. Conclusions

From this work the following conclusions are drawn:

1. In this study, a third-order Bésier curve was used to solve the Young-Laplace equation. It is known that the approximation of the third-order Bésier curve is not precise enough to calculate the meniscus of a sessile droplet on a horizontal surface. It is, therefore, desirable to use the Bésier curve of the higher-order.
2. It could not be concluded that CAs calculated for the water droplets with sizes larger larger than the capillary length differ from those calculated for the circular segment or those derived using the Cassie-Baxter equation. The effect of f_s (fraction of solid surface) on CA does not depend significantly on the droplet size, even though the droplet flattens considerably as its size increases.

Acknowledgement

Kira Lewis's original idea to use the Bézier curve method for the solution of the Young-Laplace differential equation is duly acknowledged.

Conflicts of Interest

The authors declare no conflict of interest.

References

[1] M Yamamoto, N Nishikawa, H Mayama, Y Nonomura, S Yokojima, S Nakamura, and K Uchida. Theoretical explanation of the Lotus Effect: Superhydrophobic property changes by removal of nanostructures from the surface of a lotus leaf. Langmuir. 2015, 31, 7355–7363, https://doi.org/10.1021/acs.langmuir.5b00670

[2] H Chamani, J Woloszyn, T Matsuura, D Rana, and CQ Lan. Pore wetting in membrane distillation: A comprehensive review. Progress in Materials Science. 2021, 122, 100843, https://doi.org/10.1016/j.pmatsci.2021.100843

[3] CH Kung, PK Sow, B Zahiri, and W Mérida. Assessment and interpretation of surface wettability based on sessile droplet contact angle measurement: Challenges and opportunities. Advanced Materials Interfaces, 2019, 6,1900839, https://doi.org/10.1002/admi.201900839

[4] M Yao, LD Tijing, G Naidu, SH Kim, H Matsuyama, AG Fane, and HK Shon. A review of membrane wettability for the treatment of saline water deploying membrane distillation. Desalination 2020, 479, 114312, https://doi.org/10.1016/j.desal.2020.114312

[5] RN Wenzel. Resistance of solid surfaces to wetting by water. Industrial & engineering chemistry, 1936, 28, 988–994, https://doi.org/10.1021/ie50320a024

[6] ABD Cassie and S Baxter. Wettability of porous surfaces. Transactions of the Faraday society, ,40, 546–551,https://doi.org/10.1039/TF9444000546

[7] K Seo, M Kim, and DH Kim. Re-derivation of Young's Equation, Wenzel Equation, and Cassie-Baxter Equation Based on Energy Minimization. Surface Energy. InTech. 2015, http://dx.doi.org/10.5772/61066.

[8] S. Banerjee. Simple derivation of Young, Wenzel and Cassie-Baxter equations and its interpretations. arXiv preprint arXiv:0808.1460., 2008, https://doi.org/10.48550/arXiv.0808.1460

[9] Cassie-Baxter equation, Sciencedirect. Available online; URL (accessed on 29 April 2024). https://www.sciencedirect.com/topics/engineering/cassie-baxter-equation

[10] M Liu, ZQ Wu, and DC Yin. Measurement of contact angle under different gravity generated by a long-arm centrifuge, Colloids and Surfaces A: Physicochemical and Engineering Aspects. 2020, 588, 124381, https://doi.org/10.1016/j.colsurfa.2019.124381

[11] A Baldygin, A Ahmed, R Baily, MF Ismail, M Khan, N Rodrigues, AR Salehi, M Ramesh, S Bhattacharya, T Willers, D Gowanlock, and PR Waghmare. Effect of gravity on the spreading a droplet deposited by liquid needle deposition technique, npj Microgravity. 2023, 9, 49, https://doi.org/10.1038/s41526-023-00283-2

[12] S Gulec, S Yadav, R Das, V Bhave, and R Tadmor. The influence of gravity on contact angle and circumference of sessile and pendant drops has a crucial historic aspect, Langmuir. 2019, 35, 5435-5441, https://doi.org/10.1021/acs.langmuir.8b03861

[13] Z Tang, B Xu, X Wang, and Z Chen. Effects of gravity and surface morphology on droplet contact Aangles and wetting state, Microgravity Science and Technology. 2022, 34, http://dx.doi.org/10.1007/s12217-022-09962-3

[14] K Lewis, and T. Matsuura. Calculation of the meniscus shape formed under gravitational force by solving the Young-Laplace differential equation using the Bézier curve method. ACS Omega. 2022,7, 36510-36518,https://doi.org/10.1021/acsomega.2c04359

[15] K Lewis and T Matsuura. Bézier curve method to compute various meniscus shapes. ACS Omega 2023, 8, 15371–15383, https://doi.org/10.1021/acsomega.3c00620

[16] CW Extrand and SI Moon. Contact angles of liquid drops on superhydrophobic surfaces: Understanding the role of flattening of drops by gravity. Langmuir. 2010, 26, 17090-17099, https://doi.org/10.1021/la102566c

Appendix

The functions for the cubic Bézier curve and its first and second derivatives are given as

$$B(t) = (1-t)^3 P_0 + 3(1-t)^2 t P_1 + 3(1-t)t^2 P_2 + t^3 P_3 \quad \text{(A1)}$$

$$B'(t) = 3(1-t)^2 (P_1 - P_0) + 6(1-t)t(P_2 - P_1) + 3t^2 (P_3 - P_2) \quad \text{(A2)}$$

$$B''(t) = 6(1-t)(P_2 - 2P_1 + P_0) + 6t(P_3 - 2P_2 + P_1) \quad \text{(A3)}$$

In terms of (x, y) on the rectangular coordinate,

$$x(t) = (1-t)^3 x_0 + 3(1-t)^2 t x_1 + 3(1-t)t^2 x_2 + t^3 x_3 \quad \text{(A4)}$$

$$y(t) = (1-t)^3 y_0 + 3(1-t)^2 t y_1 + 3(1-t)t^2 y_2 + t^3 y_3 \quad \text{(A5)}$$

$$x'(t) = \frac{dx}{dt} = 3(1-t)^2 (x_1 - x_0) + 6(1-t)t(x_2 - x_1) + 3t^2 (x_3 - x_2) \quad \text{(A6)}$$

$$y'(t) = \frac{dy}{dt} = 3(1-t)^2 (y_1 - y_0) + 6(1-t)t(y_2 - y_1) + 3t^2 (y_3 - y_2) \quad \text{(A7)}$$

$$x''(t) = \frac{d^2x}{dt^2} = 6(1-t)(x_2 - 2x_1 + x_0) + 6t(x_3 - 2x_2 + x_1) \quad \text{(A8)}$$

$$y''(t) = \frac{d^2y}{dt^2} = 6(1-t)(y_2 - 2y_1 + y_0) + 6t(y_3 - 2y_2 + y_1) \quad \text{(A9)}$$

Further, the derivatives $\frac{dy}{dx}$ and $\frac{d^2y}{dx^2}$ can be written as

$$\frac{dy}{dx} = \frac{\frac{dy}{dt}}{\frac{dx}{dt}} \quad \text{(A10)}$$

$$\frac{d^2y}{dx^2} = \frac{\left(\frac{dx}{dt}\right)\left(\frac{d^2y}{dt^2}\right) - \left(\frac{dy}{dt}\right)\left(\frac{d^2x}{dt^2}\right)}{\left(\frac{dx}{dt}\right)^3} \quad \text{(A11)}$$

Thus, for a given set of parameters $(x_0, x_1, x_2, x_3, y_0, y_1, y_2 \text{ and } y_3)$, we can obtain $x, y, \frac{dy}{dx}$ and $\frac{d^2y}{dt^2}$ via equations (A4) –(A11) at each *t*, that is changed from 0 to 1. *y* as a function of *x* is obtained by finding the parameters that can make the left side of equation (16), as close to zero as possible at any *t*.

It should be noted that among the 8 parameters, 4 parameters are fixed by the boundary conditions and do not subject to the change in the optimization process. Therefore, only remaining 4 parameters are considered as the adjustable parameters for optimization.